Blast actions in aircrafts: an integrated methodology for designing protection devices

Filippo Masi, Paolo Maria Mariano, Paolo Vannucci

Blast actions in aircrafts: an integrated methodology for designing protection devices

Filippo Masi[a]
Università di Firenze, via Santa Marta 3, I-50139, Firenze, Italy.

Paolo Maria Mariano[b]
DICeA, Università di Firenze, via Santa Marta 3, I-50139, Firenze, Italy.

Paolo Vannucci[c]
LMV, Université de Versailles et Saint-Quentin,
55 avenue de Paris, F-78000, Versailles, France.

We introduce a numerical approach for evaluating the response of aircraft fuselages subjected to internal explosions. We account for fluid-structure coupling through an integrated methodology able to take into account both stress at cruise altitude and blast fast-dynamics. We propose a protective device for the passenger cabin, which consists of a two-layer upholstery made of Kevlar fabric and polyurethane foam. The numerical simulations indicate the effectiveness of this device in mitigating the effect of the shock wave over the structure.

I. Introduction

We record airplane bombing attacks first in 1933 in the cargo hold of a Boeing 247D; the explosive was nytroglicerin. Table 1 presents a sequence of similar events. Until the bombing of a Boeing 707-124 in 1962, all the attacks were focused on very simple explosive devices placed in the baggage compartment. In-cabin bombs, placed mostly under seat cushions, determined most

[a] Actually, Ph.D. Student at Laboratoire Navier, École des Ponts Paris Tech, 6-8. avenue Blaise Pascal, F-77455, Marne la Vallée, France, filippo.masi@enpc.fr
[b] Professor, paolo.mariano@unifi.it
[c] Professor, paolo.vannucci@uvsq.fr

subsequent disasters. In 1987, the first liquid explosives were used, but they were rapidly replaced by plastic explosives hidden inside shoes, laptops, and other eletronic devices. The response of airlines and airports to these threats was and is focused on their prevention based on pre-board screening. Gillen and Morrison [1] report a comparative study of European total expeditures on aviation security: 5.7 billion euros in 2011.

In this context, the idea of developing the so-called *unit load devices* (ULD), a design of luggage containers with the aim of absorbing energy from an in-cargo explosion, emerged. We also record a ULD made of composite panels with reinforcing fibres [2], a bilayer hardened luggage container made of an inner layer of lightweight foam for capturing debris, and an outer pressure mitigation layer [3]. Usual protections (see e.g. [4] and [5]) consist in blowout panels incorporated into fuselages and designed to be weaker than the sorrounding airframe. In a bombing event, blowout panels will fail, allowing pressure decrement and controlled fuselage failure. In describing the process at cruise altitude, we cannot neglect pressurization and gravity loads; also, although we may suppose the absence of turbolence and wind gusts, we need to take into account the rigid body motion of the system.

A bombing event overcomes circumstances investigated in standard experiments on fuselages, usually based on a fatigue design. Experiments on the response of fuselages to a blast usually consist in an explosion inside the aircraft while it is at ground and without any acting load on it, except gravity (see [6]). The experiment presented in reference [7] considers a partially pressurized fuselage of a retired Boeing 727, while reference [8] a plane pre-pressurized panel, despite large-scale effects afflicts fuselage dynamics.

Lower-cost methods for investigating the fast-dynamics of a fuselage subjected to blast actions are computational. Several articles deal with the modelling strategies of reinforced plates in Aluminium-based alloys or glass reinforced aluminium (GLARE), (see e.g. [10]), i.e., a fibre metal laminate made of aluminium and glass fibre layers, under blast actions. A question not yet largely investigated is the behaviour of the full aircraft structure. Analyses of blast actions on fuselages, developed by adopting a Coupled-Eulerian-Lagrangian (CEL) approach, appear in references [11] and [12]. The first one deals with the effects of an in-cabin bomb placed inside the luggage compart-

ment for an Aluminium-based fuselage, assumed as a cantiveler beam. Consequently, the analysis neglects possible rigid body motions. In reference [12] the authors consider an Airbus A380 and introduce pressurization just as a static load on the skin.

In this paper, we develop a numerical approach for evaluating the response of a fuselage subjected to an in-cabin explosion, with the aim of proposing a possible passive cabin protection. The analysis includes gravity and pressurization loads at cruising altitude. We consider different volumes of air inside and outside cabin, different velocities of travelling shock waves through the volumes, and changes in pressurization.

In Section II we present the geometry of the fuselage, while in Sections III and IV we outline the way followed in representing blast actions and the constitutive behaviour of aluminium alloys, respectively. Section V deals with the development of passive protections in Kevlar and polyurethane foam. We present our numerical strategy in Section VI. Finally, in Section VII we describe the simulation of an in-cabin explosion and analyze the reliability of the proposed passive protection.

II. Fuselage geometry

We design fuselages able to hold both passengers and cargo on the basis of three different schemess: truss, monocoque, and semimonocoque.

- The truss design, commonly belonging to the first generation of aircrafts, consists of steel tubes, welded together in a framework.
- The monocoque type, i.e., *unit shell*, relies mostly on the strength of the skin (or covering) to carry loads. It consists of formers, frame assemblies, and bulkheads to provide shape with the skin carrying mainly stresses. The main problem related to such a design is keeping the weight within allowable limits while assuring enough strength.
- The semimonocoque is a modification of the latter design consisting of frame assemblies, bulkheads, and formers supplemented by additional reinforcements, called longerons, which make the structure lightweighted and stiffer. Semimonocoque fuselages are usually made of aluminium alloys, although steel and titanium are used in high temperature regions.

In the simulations presented here, we adopt the simplified semimonocoque design shown in

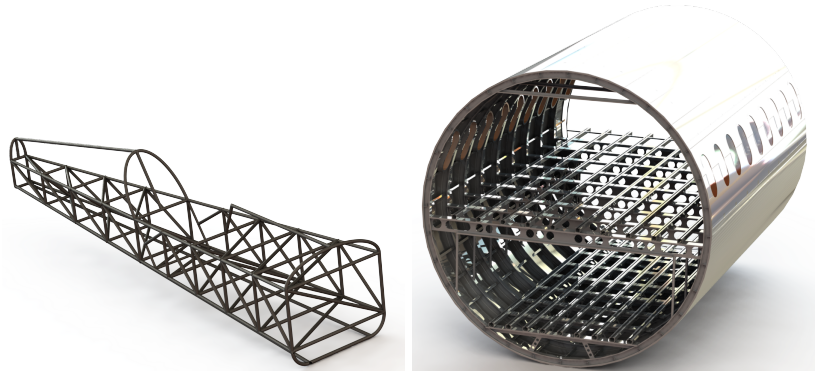

Fig. 1 Truss design (*left*) and semimonocoque design (*right*).

Figure 2. The fuselage is 4 meters long and has a diameter of 3 meters. Longerons and bulkheads appear in Figure 3, together with their sections.

The floor consists of plates with 0.8 mm thickness, while the skin has 2 mm thickness. Tied contact pairs assure continuity between different parts. Frames along the floor, longerons, and bulkheads

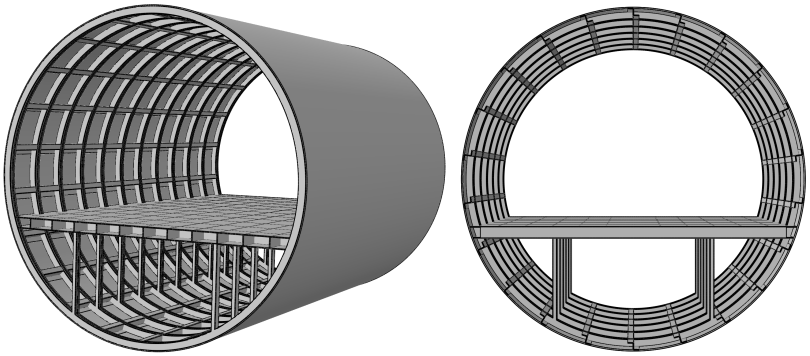

Fig. 2 The geometrical model.

are made of Al2024-T3, while the skin is made of Al7075-T6.

III. Modeling blast actions

An explosion is an extremely rapid and exothermal chemical reaction, which lasts just few milliseconds. During detonation, hot gases, pertaining to the chemical process, expand quickly and, for the hot temperatures produced almost instantaneously, the air around the blast expands too. The result is a blast shock wave, characterized by a thin zone of air propagating spherically much faster than the sound speed, through which pressure is discontinuous. We describe below more

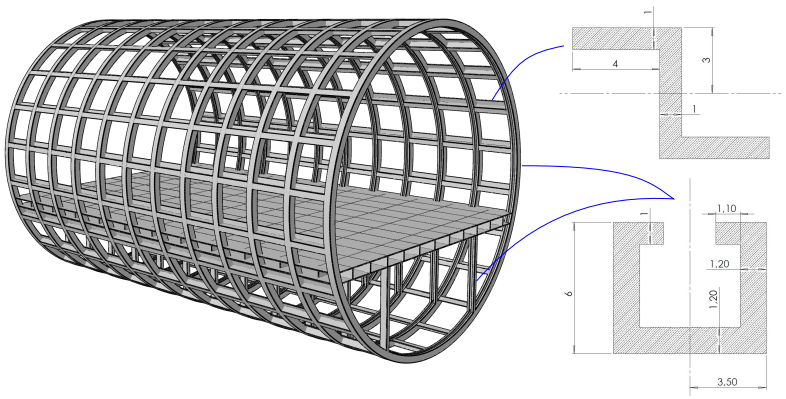

Fig. 3 Longerons and frame assemblies and related sections (measures are in millimeters).

formally such a phenomenon, more details can be found in references [13] and [14].

A few notations appear below.

- W: explosive mass.
- $R = ||q - o||$: distance of a point q from the detonation point o.
- P_o: ambient pressure.
- P_s: overpressure due to the blast; it is the pressure in the air relative to P_o.
- P_r: reflected overpressure, i.e., the pressure, relative to P_o, acting at a point q of a solid surface when hit orthogonally by a shock-wave.
- t_A: arrival time, i.e., the instant at which the shock-wave peak arrives at q.
- t_o: positive phase duration, defined below.
- t_{o-}: negative phase duration, defined below.

Figure 4 represents an ideal profile of the overpressure $P_s(q,t)$ produced by a blast. When the shock wave arrives at q, after t_A, the pressure instantaneously increases from the ambient pressure P_o to a peak for P_s: a strong discontinuity, indeed.

For $t > t_A$ the overpressure decreases exponentially until time $t_A + t_o$, when $P_s = P_o$, which marks the end of the so-called positive phase. After $t_A + t_o$, we have the negative phase: the pressure decreases with respect to P_o and comes back to P_o after $t_{o-} > t_o$. During the negative

phase the decrement of the pressure is in modulus much lower than the peak pressure of the positive phase. Consequently, the negative phase can be neglected for structural analyses, though it can be important in some special cases, due to its duration, always much longer than the positive phase. Such a behavior is idealized: perturbations can occur, due to different circumstances.

The shock wave is the main mechanical effect of a blast on a structure, but not the only one: hot gases, expanding, produce the so-called dynamic pressure, least in value with respect to the shock wave and propagating at a lesser speed, while the impinging shock wave can be reflected by solid surfaces and acts again on other surfaces as reflected shock wave.

The overpressure P_s at a point q decreases with increasing time t and distance R. Generally, the time rate decrement is much greater than the space rate one: the blast overpressure is like a localized pressure wave propagating at high speed and decreasing intensity in the distance.

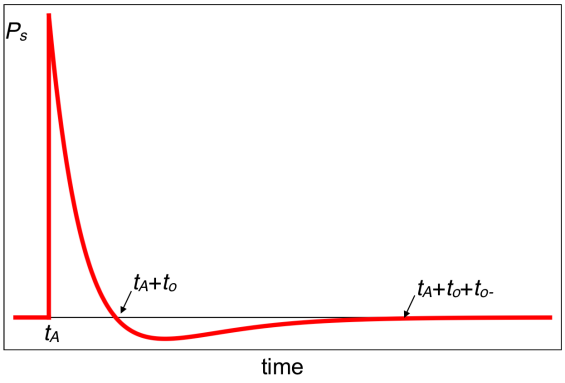

Fig. 4 Scheme of the time variation of the pressure due to a blast.

P_r is the pressure acting on a surface impinged by the incident overpressure P_s. The peak of P_r is normally much greater than the one of P_s, measured at the same point and assuming the absence of any surface.

The simulation of a blast can be conducted by using different approaches. Here we refer to three phenomenological approaches: JWL, CONWEP, and TM5-1300 models.

JWL stands for Jones, Wilkins, and Lee [15], [16], [17]. Basically, JWL rests on an equation of state, which describes the blast phenomenon including the propagation of shock-waves in a medium, its reflection on solid surfaces, and the expansion of the hot gases, i.e., the dynamic pressure. Such an equation of state expresses the overpressure P_s inside the explosive material as a function of

some parameters:

$$P_s = A\left(1 - \frac{\omega\ \rho}{R_1\rho_0}\right)\exp\left(-R_1\frac{\rho_0}{\rho}\right) + B\left(1 - \frac{\omega\ \rho}{R_2\rho_0}\right)\exp\left(-R_2\frac{\rho_0}{\rho}\right) + \omega\ \rho\ E_m. \tag{1}$$

A, B, R_1, R_2, and ω are parameters depending upon the explosive, along with ρ_0, its density, while ρ is the density of the detonation products and E_m the internal energy per unit mass. In addition, detonation velocity v_D needs to be specified. All their values are selected to fit experimental results on the cylinder expansion test (see Table 2). Equation (1) emerges from a first order expansion with respect to energy of the principal isentrope for the detonation products, i.e.,

$$P_s = A\exp\left(-R_1\frac{\rho_0}{\rho}\right) + B\exp\left(-R_2\frac{\rho_0}{\rho}\right) + C\left(\frac{\rho_0}{\rho}\right)^{-(\omega+1)}. \tag{2}$$

The principal isentrope (2) includes three different contributions, each one describing the propagation of a detonation wave inside the explosive: (i) the first exponential term accounts for the high pressure regime and dominates when the explosive is compressed, i.e., $\rho_0/\rho < 1$; (ii) the second represents the high-intermediate pressure range, i.e., $1 < \rho_0/\rho < 3 \div 4$; (iii) the last term is the equation of state of an ideal gas, $\rho_0/\rho > 4$ (see Fig. 5). JWL captures essential features of the blast phenomenon, but its drawback is the need of discretizing, finely, the charge and the fluid domain, which can be very large.

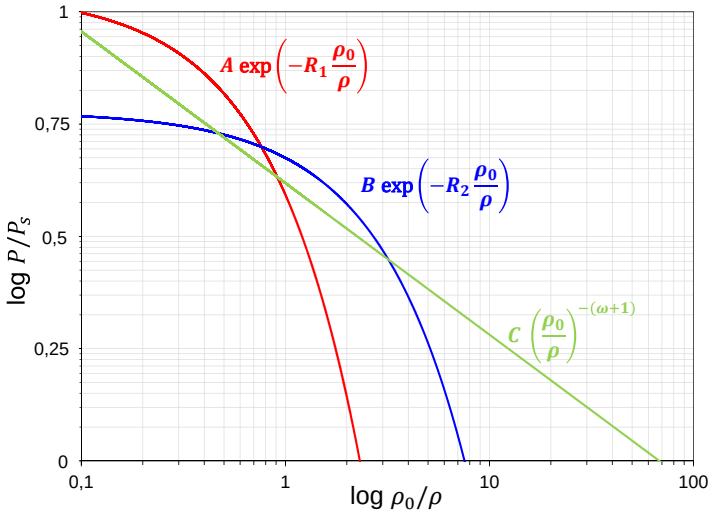

Fig. 5 Overpressure inside an explosive material, trinitrotoluene, at varying of the density of the detonation products.

We consider air as an ideal gas with total pressure given by

$$p + p_A = \rho \bar{R} T, \tag{3}$$

where p_A and p are, respectively, ambient and current (fluid) pressures; $\bar{R}$ is the universal gas constant, i.e., the product between Boltzmann and Avogadro constants; T is the current absolute temperature. We consider the specific energy, E_m, as a function of the temperature, θ, alone:

$$E_m = E_{m0} + \int_{T_0}^{T} c_v(\theta)\, d\theta, \tag{4}$$

where E_{m0} is the initial specific energy at the initial temperature T_0; c_v is the specific heat at constant volume (we assume it remains costant when temperature varies).

Multi-physics transient problems, with a strong fluid-structure coupling, lead to numerical simulations that can be very heavy. Empirical methods are often used for their reduced computational costs. The two most commonly used empirical models rest upon different but related studies of the U.S. Army Corps of Engineers (USACE): the document [20] and the Technical Manual TM5-1300 [21]. They contain the model CONWEP, completed by successive documents [22]. The Joint Research Center of the European Union has produced in 2013 a Technical Report [23] substantially referring to these two last USACE documents and to another Technical Report of the U.S. Army [24].

Such empirical models are less precise in predictions than JWL, especially because they neglect reflected waves, which may have, in contrast, prominent effects, especially for internal blasts. Depending upon geometry, the concentration of the reflected waves can give rise to local effects that can be greater than the original shock wave. In the case of vaulted structures limited laterally by walls, a localized shock wave produced by the reflected waves can hit the vault with an overpressure far greater than that produced directly by the original impinging shock wave [14], [25], [26].

In the case of aircrafts, due to the cylindrical symmetry, we can have prominent effects of focalisation. Moreover, the strong thermo-fluid-mechanics coupling requires an integrated methodology able to account for both the stress state in the structure and the evolution of the fast-dynamics explosive phenomenon. For all these reasons, we have chosen to use JWL for the numerical simulations.

IV. Aluminium alloys constitutive behaviour

For the Aluminium alloys under scrutiny we account for plastic strain, strain rate and temperature variations. Among available proposals, we refer here to Johnson's and Cook's [27] one, which includes strain hardening, strain rate and thermal softening effects. We also add the elastic component of the constitutive behaviour.

A. Plastic behaviour

Johnson-Cook's plasticity is a particular type of von Mises' plasticity with analytical form of hardening law and rate dependence.

The model expresses the static yield stress, σ^0, as a function of a nondimensional temperature, $\widetilde{T}$, and plastic small strain, $\varepsilon_{\rm pl}$, as

$$\sigma^0 = \left[JC_1 + JC_2\left(\varepsilon_{\rm pl}\right)^n\right]\left(1-\widetilde{T}^m\right), \tag{5}$$

where JC_1 is the yield strength, while JC_2 and n are, respectively, the hardening constant and an exponent to be determined on the basis of data fitting; m is the thermal softening exponent, and $\widetilde{T}$ is defined by

$$\widetilde{T} = \begin{cases} 0 & \text{if } T < T_{\rm tr} \\ (T-T_{\rm tr})/(T_{\rm m}-T_{\rm tr}) & \text{if } T_{\rm tr} \le T \le T_{\rm m} \\ 1 & \text{if } T > T_{\rm m} \end{cases} \tag{6}$$

where $T_{\rm m}$ is the melting temperature and $T_{\rm tr}$ is the transition temperature defined as the one at which the yield stress is temperature-independent. If $T > T_{\rm m}$, $\sigma^0 = 0$: the material would melt. However, Johnson-Cook's constitutive relation is not completely appropriate in analyses where temperature is higher than the material recrystallization threshold, due to the presence of microstructural changes such as decreasing dislocation density and increasing grain size.

The yield stress at non-zero strain is given by

$$\sigma_Y = \left[JC_1 + JC_2\left(\varepsilon_{\rm pl}\right)^n\right]\left[1 + JC_3 \ln\left(\frac{\dot{\varepsilon}_{\rm pl}}{\dot{\varepsilon}_0}\right)\right]\left(1-\widetilde{T}^m\right). \tag{7}$$

B. Damage

Damage growth δ satisfies the rule

$$\delta = \sum_{k=0}^{k=K} \frac{\Delta\varepsilon_{\mathrm{pl},k}}{\varepsilon_{\mathrm{pl},f}}, \tag{8}$$

where $\Delta\varepsilon_{\mathrm{pl}}$ is an increment of the equivalent plastic strain, $\varepsilon_{\mathrm{pl},f}$ the strain at failure and K the total number of increments in the analysis. By assumption, the strain at failure is given by

$$\varepsilon_{\mathrm{pl},f} = \left[d_1 + d_2 \exp\left(d_3 \frac{p}{q}\right)\right]\left[1 + d_4 \ln\left(\frac{\dot{\varepsilon}_{\mathrm{pl}}}{\dot{\varepsilon}_0}\right)\right]\left(1 + d_5 \widetilde{T}\right), \tag{9}$$

where p indicates pressure, q Mises stress and d_i, $i = 1, \ldots, 5$, are failure parameters.

Tables 4 and 5 show the pertinent parameters for Al7075-T6 and Al2024-T3.

V. Passive protections

Laminated composites are often used in aeronautics since they are lightweigth materials with excellent mechanical properties. For their high toughness, aramidic fibres are usually adopted in aerospace engineering and ballistic applications. Indeed, unlike glass and carbon fibers, when Kevlar fibers break, they fail by a series of energy absorbing fibril failures and not by a brittle cracking, where fibrils are sub-fibers that compose each aramidic fiber.

Kevlar fabric properties make it a candidate to be used in designing blast-protections in the case of a fuselage. A cabin load device (CLD) to mitigate blast waves from an explosion consists in inserting Kevlar fabric inside the passenger cabin, tied with longerons and bulkheads, upholstering the interiors. During an explosion, while experiencing large strain, CLD may protect the skin and prevent from fuselage perforation, as we shall see in Section VII. In a sense, the contribution of a Kevlar-made CLD can be regarded as an increment of the viscosity of the medium through which blast waves propagate.

An improvement of the CLD protection can be obtained using foam in cavities of the fuselage such as the spaces between longerons and the interior of the floor. Foams, as energy absorbing materials, allow to mitigate the stresses due to impact, being characterised, at the same time, by low densities. Polyurethane foams are excellent candidates for blast protections.

A. Kevlar

We assume for Kevlar fabric an orthotropic elastic behaviour up to failure. Also, we consider a plane stress state ($\sigma_{13} = \sigma_{23} = \sigma_{33} = 0$). With σ the Cauchy stress tensor, ε the total elastic strain, and D the fourth-rank elasticity tensor, the standard linear elastic constitutive relation reads

$$\sigma = \mathrm{D}\,\varepsilon \tag{10}$$

With E_i Young moduli, ν_{ij} Poisson ratios, and G_{ij} shear moduli, $i, j = 1, 2, 3$, in Voigt's notation, with $\gamma_{ij} = 2\epsilon_{ij}$, relation (10) writes

$$\begin{Bmatrix} \varepsilon_{11} \\ \varepsilon_{22} \\ \gamma_{12} \end{Bmatrix} = \begin{bmatrix} 1/E_1 & -\nu_{21}/E_2 & 0 \\ -\nu_{12}/E_1 & 1/E_2 & 0 \\ 0 & 0 & 1/G_{12} \end{bmatrix} \begin{Bmatrix} \sigma_{11} \\ \sigma_{22} \\ \sigma_{12} \end{Bmatrix} \tag{11}$$

and

$$\varepsilon_{33} = -\frac{\nu_{13}}{E_1}\sigma_{11} - \frac{\nu_{23}}{E_2}\sigma_{22} \neq 0 \tag{12}$$

The elastic parameters, collected in Table 6, refer to a woven fabric Kevlar-29 with a polyvinyl-butyral-phenolic matrix, with 18% of fibers volume fraction.

We consider Hashin's failure criterion for fiber-reinforced materials [33]. In this way we account for four different damage mechanisms: fiber tension and compression, matrix tension and compression. The initiation criterion relies on a set of damage variables, each one corresponding to a damage

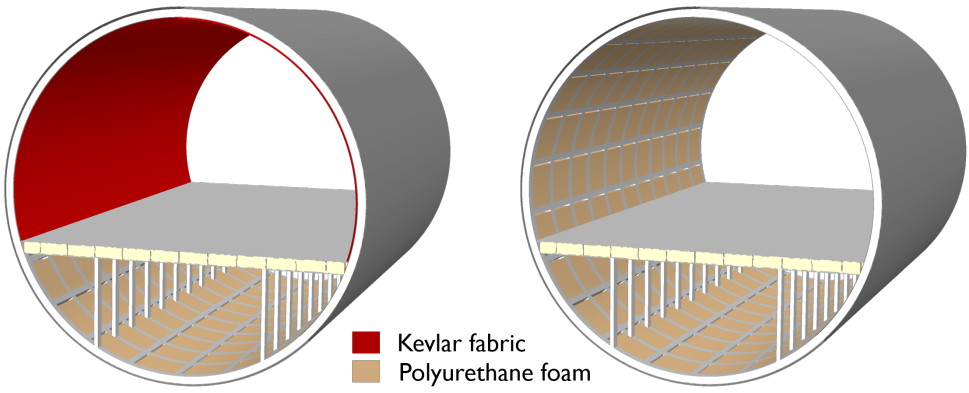

Fig. 6 CLD and covering in polyurethane foam.

mechanism:

$$d_f^t = \left(\frac{\widehat{\sigma_{11}}}{X^t}\right)^2 + \left(\frac{\widehat{\sigma_{12}}}{S^l}\right)^2, \tag{13}$$

$$d_f^c = \left(\frac{\widehat{\sigma_{11}}}{X^c}\right)^2, \tag{14}$$

$$d_m^t = \left(\frac{\widehat{\sigma_{22}}}{Y^t}\right)^2 + \left(\frac{\widehat{\sigma_{12}}}{S^l}\right)^2, \tag{15}$$

$$d_m^c = \left(\frac{\widehat{\sigma_{22}}}{2S^t}\right)^2 + \left[\left(\frac{Y^c}{2S^t}\right)^2 - 1\right]\frac{\widehat{\sigma_{22}}}{Y^c} + \left(\frac{\widehat{\sigma_{12}}}{S^l}\right)^2, \tag{16}$$

where X^t and X^c are, respectively, longitudinal tensile and compressive strengths; Y^t and Y^c transverse tensile and compressive strengths; S^l and S^t in-plane and transversal shear strengths; $\widehat{\sigma_{11}}$, $\widehat{\sigma_{22}}$ and $\widehat{\sigma_{12}}$ the components of the effective stress tensor computed by

$$\widehat{\sigma} = \mathrm{M}\sigma, \tag{17}$$

where M is the damage operator, which we assume to be

$$\mathrm{M} = \begin{bmatrix} 1/(1-d_f) & 0 & 0 \\ 0 & 1/(1-d_m) & 0 \\ 0 & 0 & 1/(1-d_s) \end{bmatrix}. \tag{18}$$

d_f, d_m and d_s are damage variables associated with fiber, matrix and shear modes, respectively, namely

$$d_f = \begin{cases} d_f^t & \text{if } \widehat{\sigma_{11}} \geq 0 \\ d_f^c & \text{if } \widehat{\sigma_{11}} < 0 \end{cases} \tag{19}$$

$$d_m = \begin{cases} d_m^t & \text{if } \widehat{\sigma_{22}} \geq 0 \\ d_m^c & \text{if } \widehat{\sigma_{22}} < 0 \end{cases} \tag{20}$$

$$d_s = 1 - \left(1-d_f^t\right)\left(1-d_f^c\right)\left(1-d_m^t\right)\left(1-d_m^c\right) \tag{21}$$

In Table 7 the parameters of Hashin's failure criterion are collected, together with the fracture energy G_f [34], assumed to be equally distributed in the longitudinal, transverse and shear directions.

B. Polyurethane foam

As usual, we consider polyurethane as a visco-elastic material with null Poisson ratio and a density of 240 kg/m^3. Data about the constitutive coefficients derive from uniaxial tension and compression tests, at different strain rates [35]. We neglect failure in compression and assume a maximal value of 3.8 MPa of the maximum principal tensile stress, independently of the strain rate.

VI. Numerical procedure

We simulate an in-cabin explosion by using a CEL approach: the fuselage is immersed into air; we use JWL to model the blast.

In CEL simulations, ABAQUS/Explicit takes into account the Eulerian fluid domain through the so-called volume-of-fluid-method: the flow through the mesh is tracked by the definition of an additional variable within each element, the Eulerian volume fraction (EVF). In our case, this allows to compute not only the propagation of shock waves, but also the diffusion of the explosive inside the air domain. We describe fluid-structure interaction by using a general contact algorithm, with a null interface friction coefficient and a penalty method.

As already pointed out in Section I, the complex nature of the loads acting on an aircraft needs to be considered by taking into account the pre-bombing stress state in a fuselage at cruising altitude. With this in mind, we propose a methodology of analysis based on two steps:

- First, through a quasistatic analysis we apply incrementally gravity and a distributed load equivalent to lift, acting on the lower half of the fuselage. Figure 7 shows the boundary conditions, which allow a rigid body motion as soon as the equilibrium between vertical loads is broken.

- The results are the initial state of a subsequent simulation where pressurization load appears through a gradient of pressure between internal and external volumes of air, using a CEL approach. We assume the aircraft at an altitude of 10000 m, while the equivalent effective cabin altitude is 2000 m.

Figure 8 shows the scheme of the procedure described above. We use the stress state obtained from the second analysis as initial state of the simulations of an internal explosion at cruising

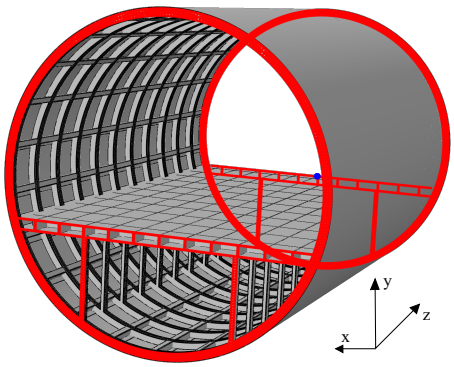

Fig. 7 Symmetric boundary conditions (*red*) along z axis applied in every analysis and no x-translation boundary condition (*blue*) applied in the CEL-CTD analysis.

altitude.

The size of the problem and the thermal sensitive behaviour of Al-alloys require considering the blast heat release. To this aim we use a Coupled-Temperature-Displacement (CTD) analysis. The equilibrium state achieved at the end of the second analysis is the initial state of a CEL-CTD explicit analysis for studying the effects of blast waves on the structure. The state equations for explosive and air are those already shown in Table 2.

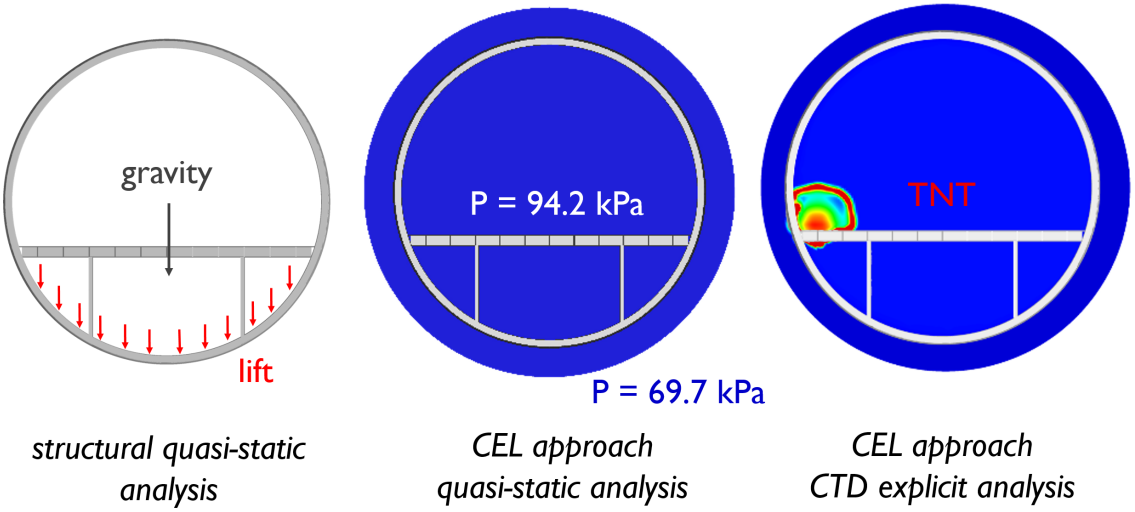

Fig. 8 Schematic representation of the procedure proposed for evaluating the stress state of the structure.

A. Mesh sensitivity of the fluid domain

The air domain is shown in Figure 9. It is decomposed into 1.156×10^6 8-nodes hexaedral volume elements, for 5.78×10^6 degrees of freedom (DOF). Boundary conditions consist on nonreflecting

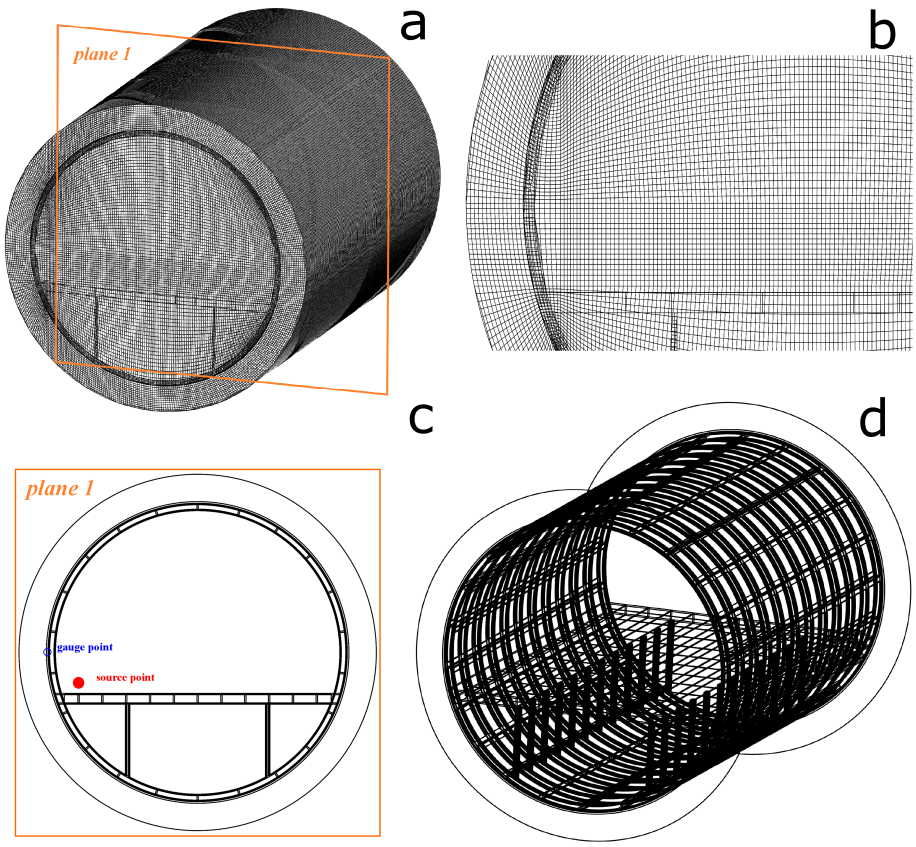

Fig. 9 The air domain: a) complete mesh M_5, b) detail of the mesh M_5, c) location of the gauge and source points, d) overall view.

outflow conditions, applied to the whole boundary.

We subdivide the considered cylindrical air domain into two different volumes: the one inside the fuselage and an exterior one corresponding to a cylinder with a diameter of 4 m.

The mesh fineness follows from a convergence analysis. We have considered six different meshes for the air domain: from the coarsest, M_1, with 0.58×10^6 DOF, to the finest one, M_6, with 10.54×10^6 DOF. For each mesh, we have computed the blast overpressure due to an explosive charge placed in the middle of the fuselage length, identified by the plane 1, in correspondence of the gauge point, highlighted in Figure 9.

In Figure 10 we show the relative error evaluated for meshes $\mathrm{M}_1, \ldots, \mathrm{M}_5$ with respect to mesh M_6; such an error, in percent, is

$$err = 100 \left| \frac{p_{M_i} - p_{M_4}}{p_{M_4}} \right|, \tag{22}$$

where p_{M_i} is the peak overpressure in the gauge point evaluated for grid M_i, while p_{M_6} is the same for the reference mesh M_6. After the evaluation of the results, we have selected the mesh M_5, with 5.72×10^5 DOF.

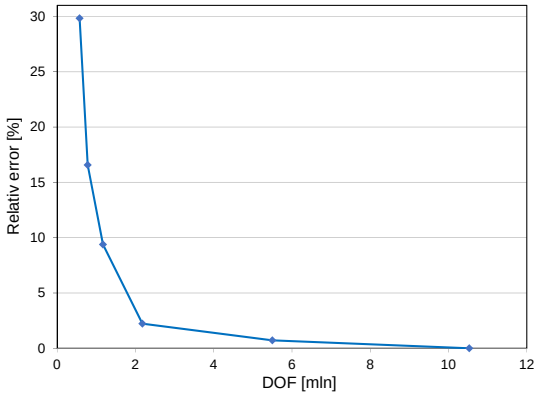

Fig. 10 Relative error, eq. (22), for the gauge point as function of the number of DOF.

B. Mesh sensitivity of the structural domain

Once the grid for the fluid domain has been selected, we have perfomed a convergence analysis for corroborating the choice of the fuselage mesh, made of four-nodes thermally coupled shell elements, supported by the explicit solver of ABAQUS.

The convergence analysis rests on two quasistatic analyses. As already pointed out, first we consider gravity and lift loads. Then, the equilibrium state enters a second analysis in which we consider the fluid domain, discretized with the selected mesh M_5, and we apply the pressurization load.

The convergence analysis rests on explicit schemes for nine different structural meshes MS_i, $i = 1, \ldots, 9$, with characteristics in Table 8.

We have monitored the values of strain at a point belonging to the skin, as shown in Figure 11. The need of evaluating the degree of accuracy of the mesh in terms of strains instead of displacements

is a consequence of rigid body motions of the structure.

We have evaluated convergence as for the air domain, computing for each mesh MS_i, with $i = 1, \ldots, 8$, the errors $\Delta\varepsilon$ of the strain magnitude ε, relatively to the same quantity ε^r, calculated for the reference mesh MS_9, the finest one:

$$\Delta\varepsilon = \left| \frac{\varepsilon - \varepsilon^r}{\varepsilon^r} \right|, \tag{23}$$

for any mesh MS_i.

In Figure 11 we show the diagram of $\Delta\varepsilon$ versus DOF. After the evaluation of the results, we have selected the mesh MS_8 for the final simulations. A detail of the structural mesh MS_8 appears in Figure 12.

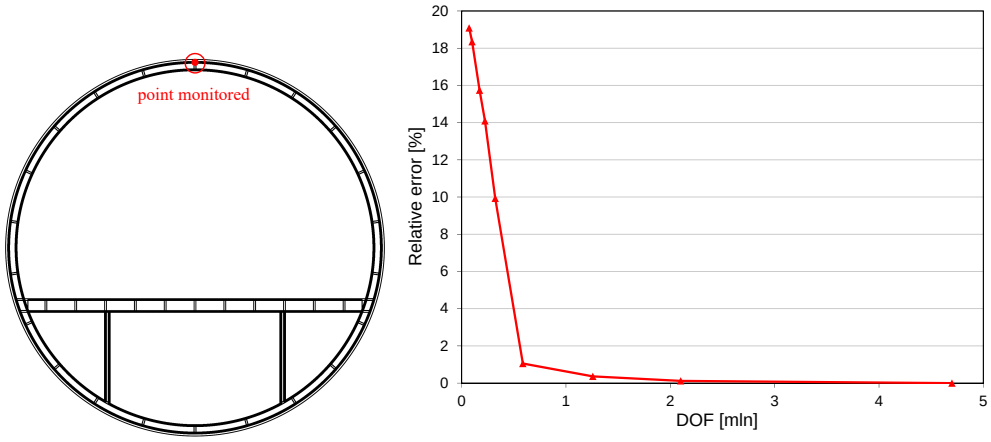

Fig. 11 Relative error $\Delta\varepsilon$ versus DOF, with respect to a point of the skin.

We use parallel computing for decreasing significantly computational time. All the simulations exploited a 24-cores workstation.

VII. Numerical simulations

We have simulated a blast, produced by the explosion of 0.850 kg TNT equivalent in-cabin charge, through a CEL-CTD analysis. From these results we have designed a CLD, Fig. 6. The stable time step of the explicit schemes, mostly afflicted by the small elements size (see [30]) varies from 2.9×10^{-7} s to 5.7×10^{-11} s. Therefore, the computational time required for running a short time period (3.5 milliseconds) analysis is around 35 hours.

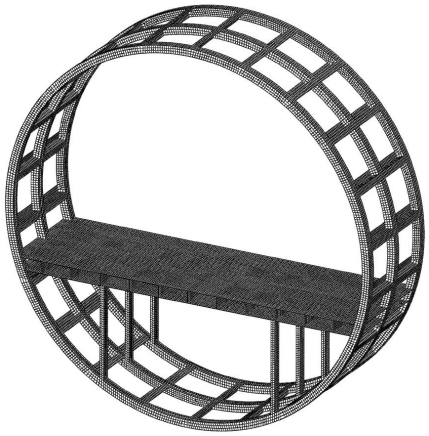

Fig. 12 Detail of the structural mesh MS_8.

A. In-cabin explosion simulations

Figures 13, 14 and 15 show the results of the simulations. The evolution of the pressure field thorugh the air domain is in Figure 13.

The blast event is really fast and the response of the fuselage can be easily seen in a really short time period, such as 3 milliseconds. The state of structural damage at the end of the calculations is in Figure 14, while the progressive response of bulkheads, longerons and skin to the blast is in Figure 15. The results confirm that a small amount of charge, capable just of piercing the skin at sufficently high altitude, can be the origin of a disaster. The principal shock front produces a hole in the skin enlarged by the subsequent decompression until global failure. The overpressure, responsable for destroying the skin in the immediate proximity of the charge, punctures also the floor (see Fig. 13), determining a secondary shock, which propagates inside the cargo hold and opens another hole in the bottom half of the skin by venting.

B. Assessing the reliability of the protective CLD

Figure 16 shows the evolution of the pressure field in the air domain considering the protective CLD: we get mitigation of blast waves, thanks to both materials and the way the protections are inserted. By comparing Figures 16 and 13, we can see the advantages of using a Kevlar fabric as a result of the smooth evolution of the principal shock front and reflected waves with a lower magnitude. Indeed, such a fabric behaves like a second skin, much less stiff and tougher than the

one made of Al7075-T6. Its main effect is a reduction of the magnitude of reflected blast waves.

Figures 17 and 18 shows the structural damage and the progressive response of fuselage and CLD, respectively. Skin can withstand an internal explosion of 0.850 kg, being not punctured, and floor is only partially damaged, avoiding the failure of the bottom half skin, due to venting, as shown in Figure 16, where any blast wave penetrates inside the cargo hold.

Figure 19 shows the comparison between the results of an in-cabin explosion without any protecting devices and those where a CLD is considered.

We have also investigated the efficacy of the protective device in the case of an explosive charge of 1 kg, as well. Figures 20, 21, and 22 show the damage for both cases, with and without protections.

C. Further remarks

Numerical simulations dealing with the behaviour of fuselages under blasts are usually based on the application of pressurization load as a distributed action on the skin independently of the pressures of the surrounding volumes of air; this hypothesis is investigated in the Appendix.

The simulations presented here allow to capture the fast-dynamics due to an internal explosion. The difference between numerical results and reality requires reliable experimental tests. However, our results furnish indication addressing towards a reasonably profitable design.

Table 1 Airliner bombing attacks, from [9].

Date	Flight	Description	Casualities
1933	Boeing 247D, United Air Lines	bomb made of nytroglicerin placed in the baggage compartment	7
1949	Douglas C-47-DL, Canadian Pacific Airlines	bomb made of dynamite placed in the baggage compartment	23
1955	Douglas DC-6B, United Air Lines	bomb made of dynamite	44
1962	Boeing 707-124, Continental Air Lines	explosive device inside passenger cabin	45
1966	Douglas RD4-1, Aden Airlines	explosive device inside passenger cabin	30
1967	DH-106 Comet 4, British European Airways	high explosive device within the cabin under seats	66
1970	Convair CV-990-30A-6 Conorado, Swissair	bomb in the baggage compartment	47
1976	Douglas DC-8-43, Cubana de Aviación	explosive device at the rear of the cabin	73
1976	Boeing 720-023B, Middle East Airlines	bomb in the baggage compartment	81
1982	Boeing 747-121, Pan Am	bomb placed under a seat cushion	1
1985	Boeing 747-237B, Air India	high explosive device inside the cargo compartment	329
1986	Boeing 727-231, Trans World Airlines	explosive device in the cabin	4
1986	Boeing 737-270C, Iraqi Airways	two hand grenades in the cabin	63
1987	Boeing 707-3B5C, Korean Air	liquid explosives concealed as liquor bottles	115
1988	Boeing 747-121, Pan Am	high-explosive device in the cabin	270
1989	McDonnel Douglas DC-10-30, Union de Transport Aériens	high explosive device in the cargo hold	170
1989	Boeing 727-21, Avianca Airlines	explosive near the fuel tank	110
2001	Boeing 767, American Ailines	plastic explosive concealed within shoes	0
2004	Tupolev Tu-134-3, Volga-Avia Express Tupolev Tu-154B-2, Siberia Airlines	high explosive devices	90
2015	Airbus A32-231, Metrojet	1 kg of TNT	224
2016	Airbus A321-111, Daallo Airlines	explosive device concealed within a laptop computer	1

Table 2 Physical parameters for the state equations for air an explosive, after [18] and [19].

AIR	ρ	Temperature	Gas constant	Specific heat				
	[kg/m^3]	[K]	[J/(kg K)]	[W/(m K)]				
	1.225	288.2	287.058	717.6				
TNT	ρ_0	v_D	A	B	ω	R_1	R_2	E_m
	[kg/m^3]	[m/s]	[MPa]	[MPa]				[kJ/kg]
	1630	6930	373770	3747.1	0.35	4.15	0.9	3680

Table 3 Material elastic and thermal parameters.

Material	ρ	E	ν	Specific heat	Thermal conductivity
	[kg/m^3]	[GPa]		[J/(kg K)]	[W/(m K)]
Al7075-T6	2810	71.7	0.33	848	130
Al2024-T3	2770	73.1	0.33	863	121

Table 4 Material parameters for Johnson-Cook's plasticity (according to [28] and [29]).

Material	JC_1	JC_2	n	m	JC_3	T_{tr}	T_{m}	$\dot{\varepsilon}_0$
	[MPa]	[MPa]				[K]	[K]	[1/s]
Al7075-T6	517	405	0.41	1.1	0.0075	292.2	750	0.000161
Al2024-T3	265	426	0.34	1.0	0.015	293.2	775	1.0

Table 5 Material parameters for Johnson-Cook's damage (according to [28] and [29]).

Material	d_1	d_2	d_3	d_4	d_5	Elongation at break
						[%]
Al7075-T6	0.005	0.34	-1.5	-0.039	8	22
Al2024-T3	0.13	0.13	-1.5	0.011	0	18

Table 6 Material parameters for Kevlar fabric (according to [31] and [32]).

ρ	E_1	E_2	G_{12}	ν_{12}
[kg/m^3]	[GPa]	[GPa]	[GPa]	
1230	18.5	18.5	0.77	0.25

Table 7 Material parameters for Hashin's failure criterion [32].

X^t	X^c	Y^t	Y^c	S^t	S^l	G_f
[MPa]	[MPa]	[MPa]	[MPa]	[MPa]	[MPa]	[kJ/m^2]
555	555	34.5	34.5	898	77	1.64

Table 8 Characteristics of the studied structural meshes.

Mesh	Average element size $[cm]$	Number of elements	Number of DOF $[mln]$
MS_1	10	9191	7.23×10^{-2}
MS_2	8	12520	1.01×10^{-1}
MS_3	6	21329	1.73×10^{-1}
MS_4	5	27971	2.24×10^{-1}
MS_5	4	40813	3.22×10^{-1}
MS_6	3	74611	5.87×10^{-1}
MS_7	2	159764	1.26
MS_8	1.5	266811	2.10
MS_9	1	5597159	4.7

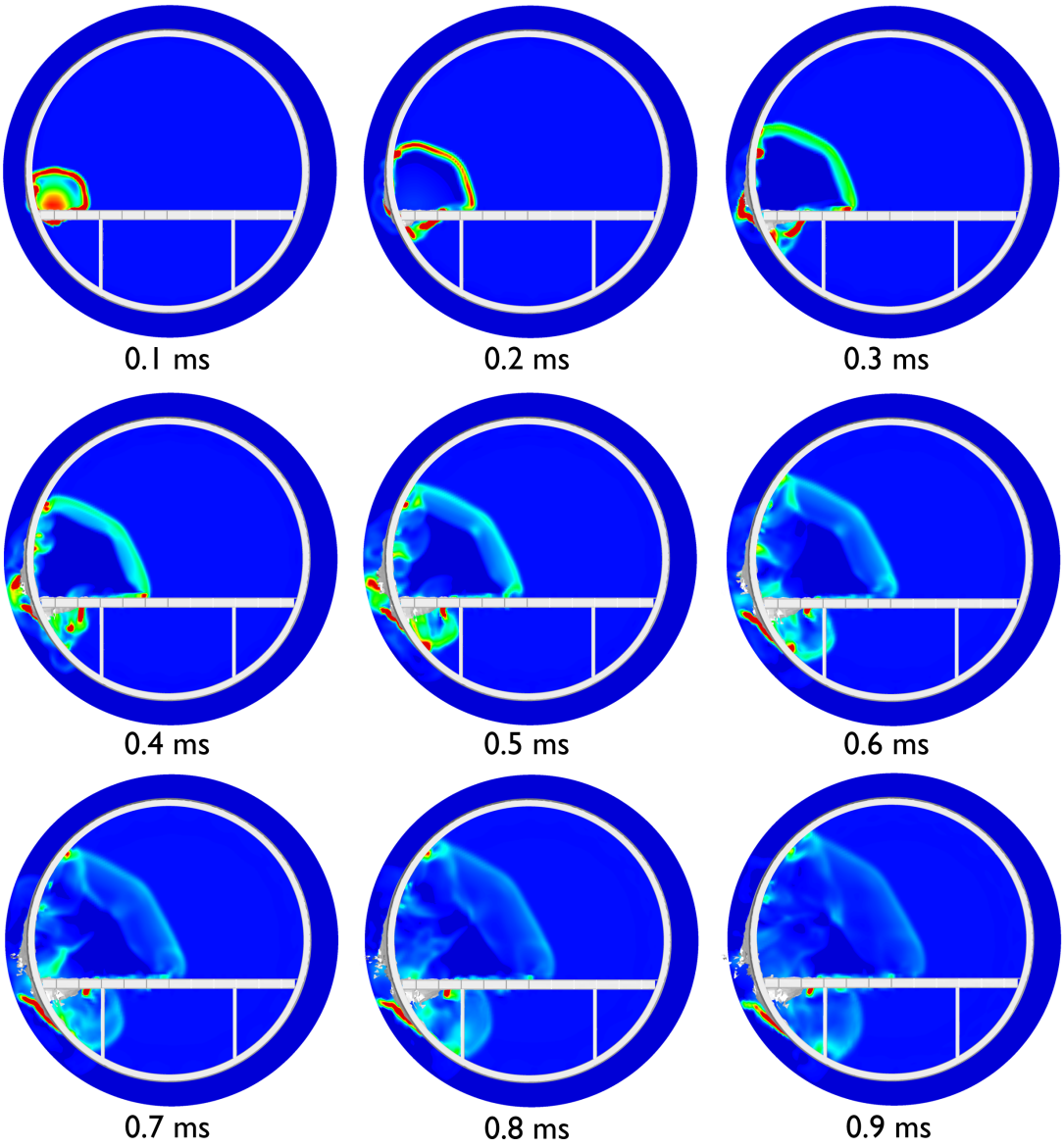

Fig. 13 The evolution of the pressure field through the air domain.

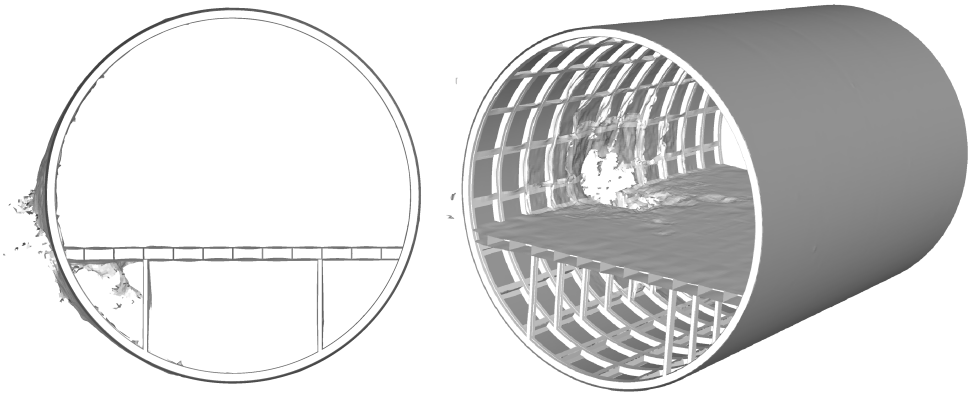

Fig. 14 Stuctural damage at the end of the calculations.

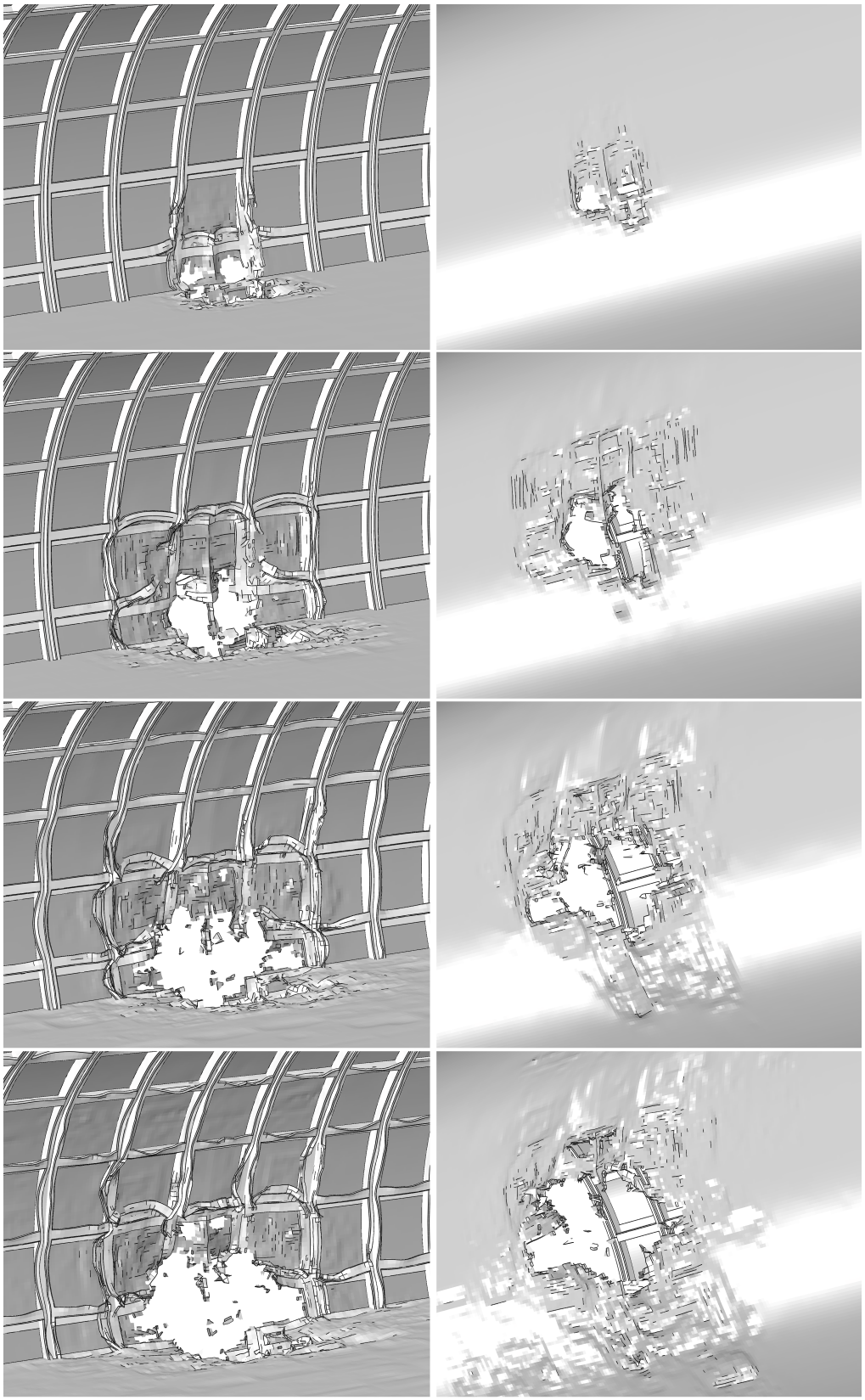

Fig. 15 Simulation of an internal blast: internal (*left*) and external views (*right*).

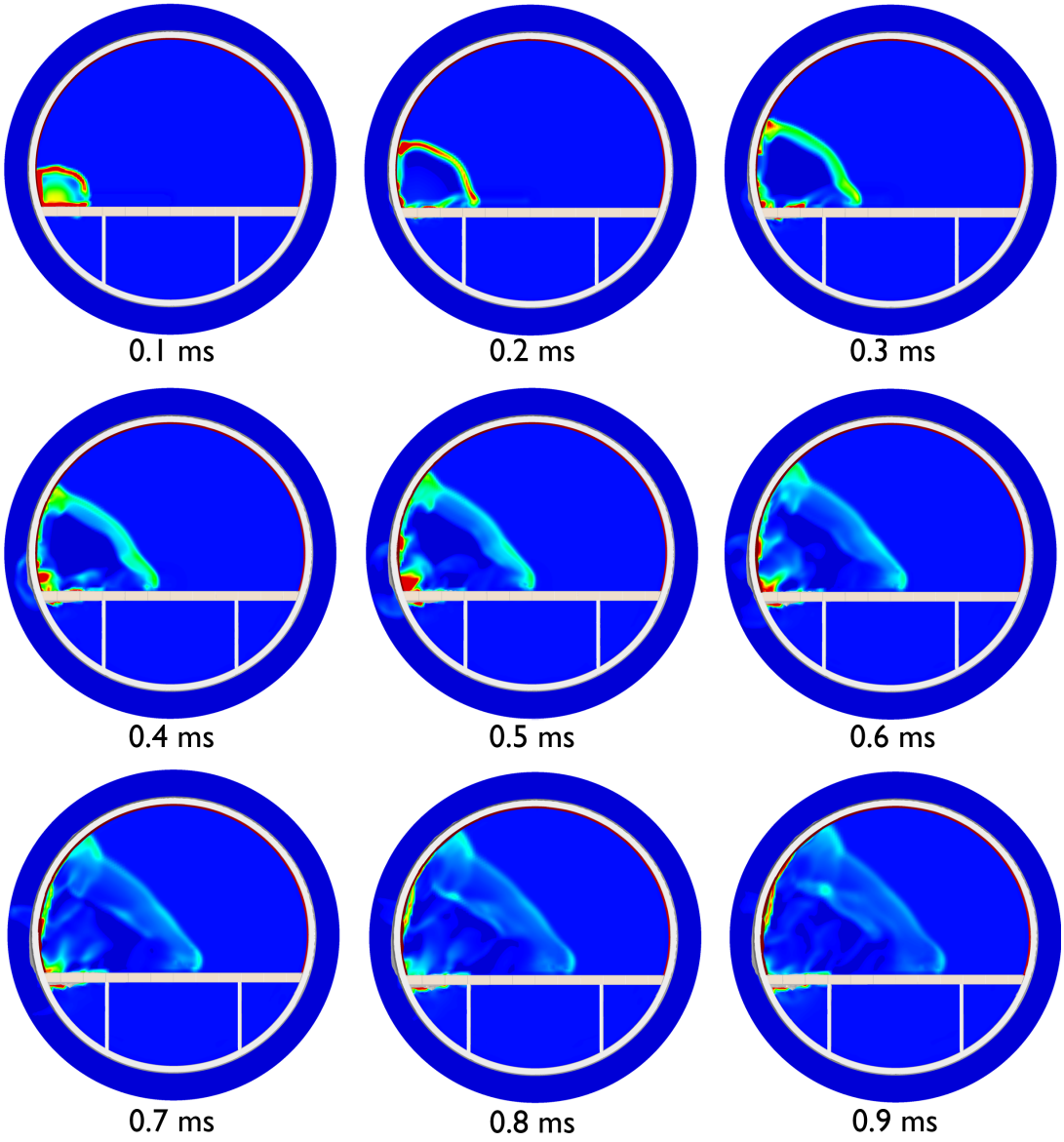

Fig. 16 The evolution of the pressure field through the air domain, with CLD.

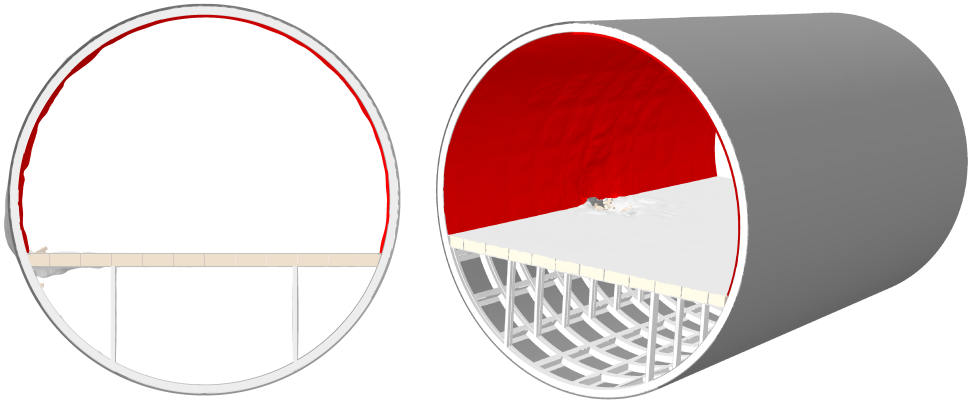

Fig. 17 Stuctural damage at the end of the calculations, with CLD.

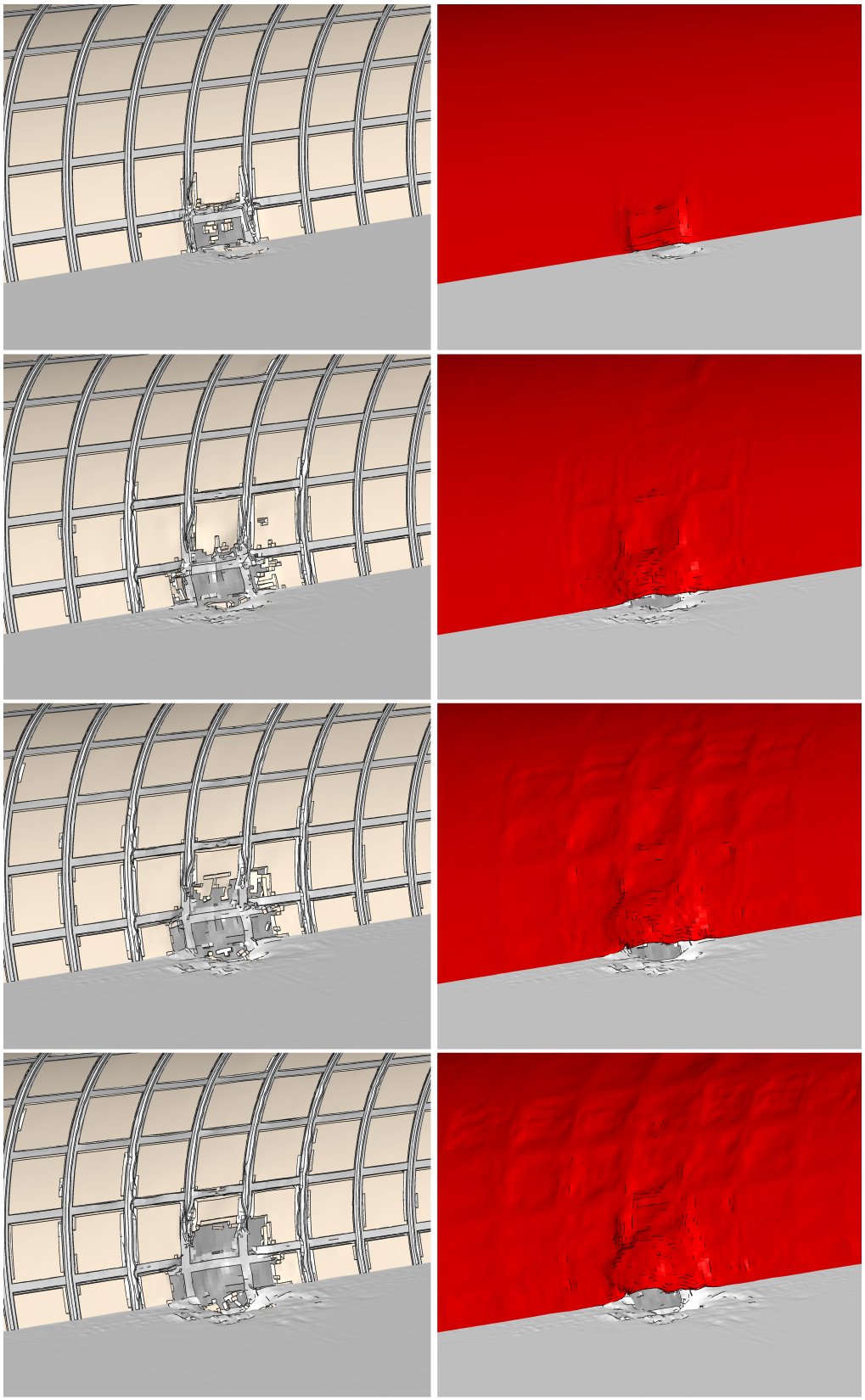

Fig. 18 Simulation of an internal blast with CLD.

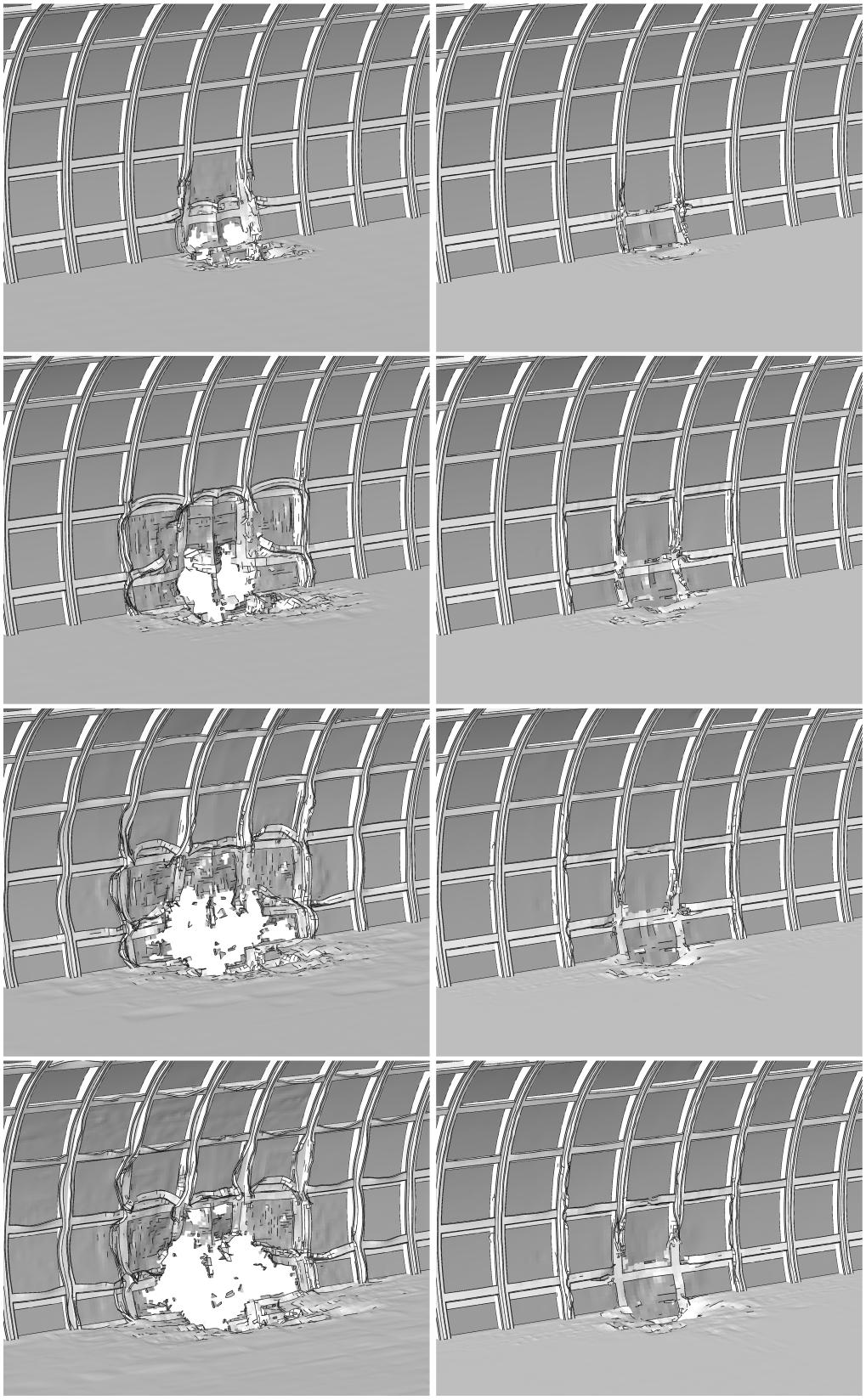

Fig. 19 Comparison between the reference design (*left*) and the CLD (*right*), foam and Kevlar fabric are not displayed.

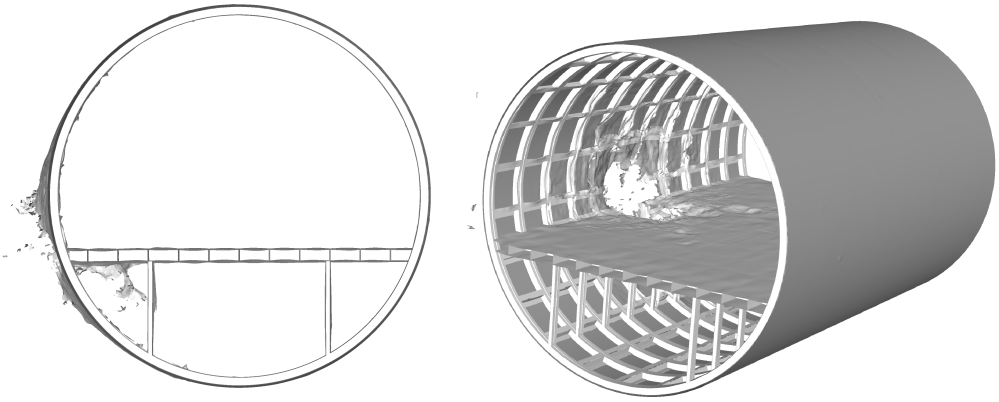

Fig. 20 Stuctural damage at the end of the calculations (W = 1 kg).

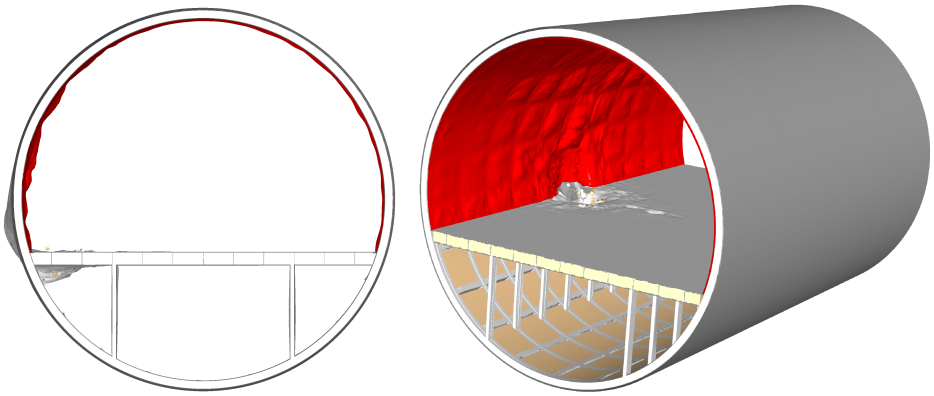

Fig. 21 Stuctural damage at the end of the calculations, with CLD (W = 1 kg).

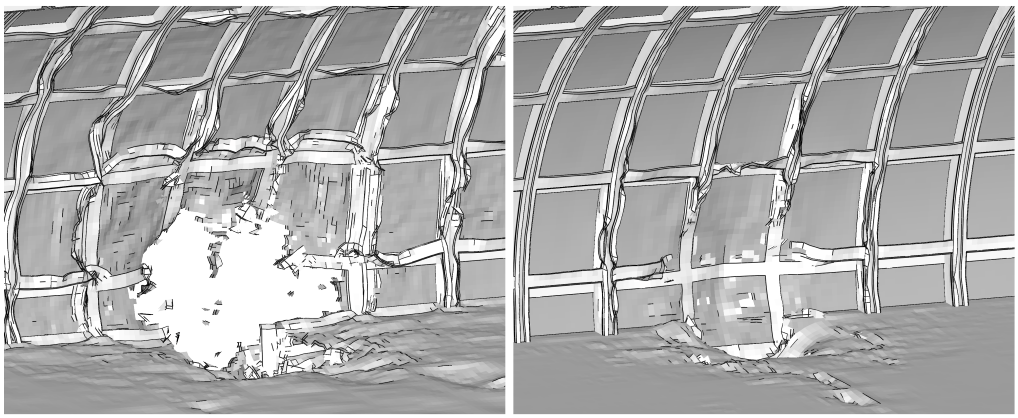

Fig. 22 Comparison between the reference design (*left*) and the CLD (*right*), foam and Kevlar fabric are not displayed (W = 1 kg).

Appendix

We analyze here the pressurization load by comparing two different schemes. In reference [12] the stresses due to pressurization emerges from the application of a distributed load, acting perpendicularly on the internal side of the skin, equivalent to the difference in pressure between inside and outside the cabin. Differently, the investigations presented in Section VII rely on the evaluation of pressurization by applying two different values of pressure to the internal and surrounding volumes of air. The two different ways of accounting for pressurization are in Figure 23.

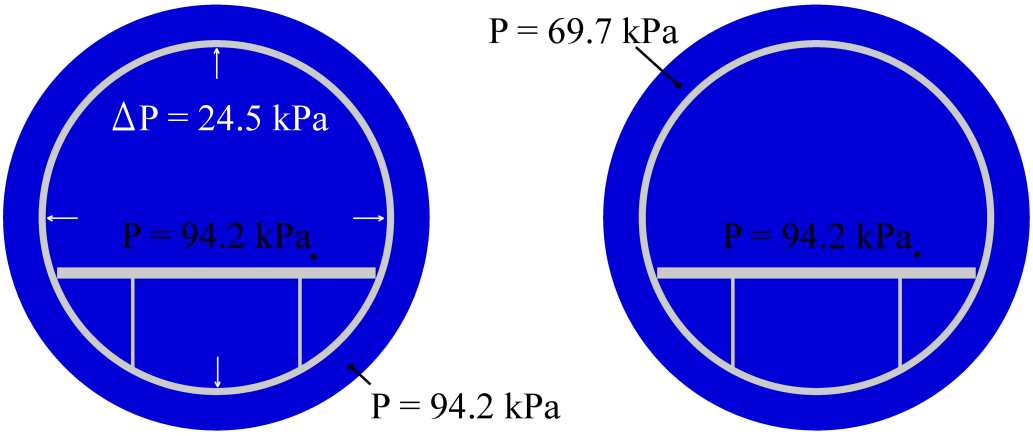

Fig. 23 Different pressurization loads; (a) same value of pressure applied in the all air domain plus a continuous load equivalent to the diffence between internal and external atmospheric pressures (*left*), (b) distinction between the internal and external values of the pressure (*right*).

Modeling pressurization through a uniformly distributed dead load, case (a), is questionable when skin breaks. Indeed, when a hole occurs, the cabin undergoes decompression. In contrast, when we apply pressurization by distinguishing the pressure values in the internal and external volumes of air, we may take into account decompression.

In order to evaluate the difference between the two ways of modeling pressurization, we develop a numerical simulation with a charge of 0.5 kg for both cases. The comparison appears in Figures 24 and 25. Case (a) leads to a more severe damage of the fuselage, due to the constant pressure acting on it. Case (b) does not lead to skin perforation.

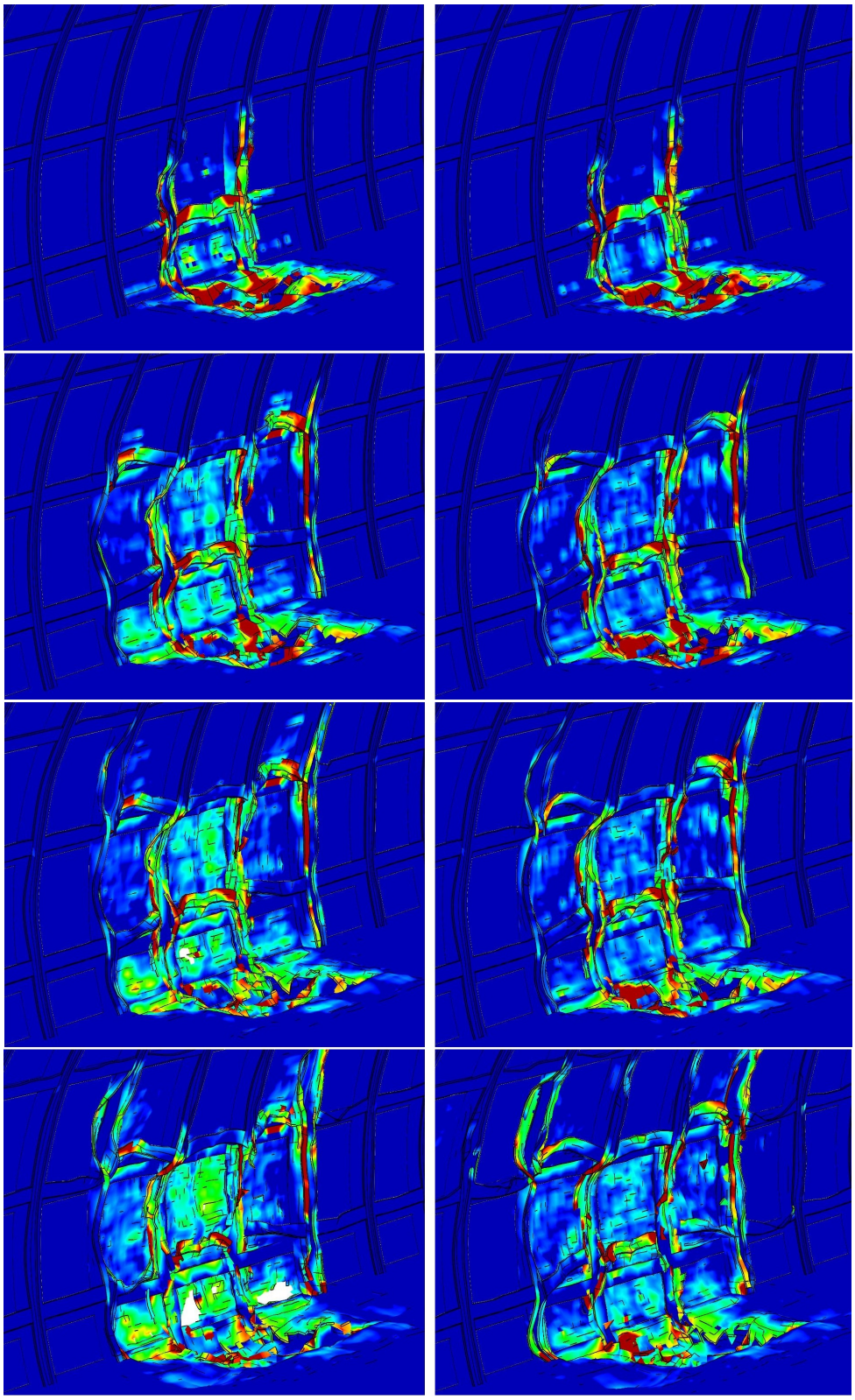

Fig. 24 Equivalent plastic strain: case (a) (*left*) and case (b) (*right*).

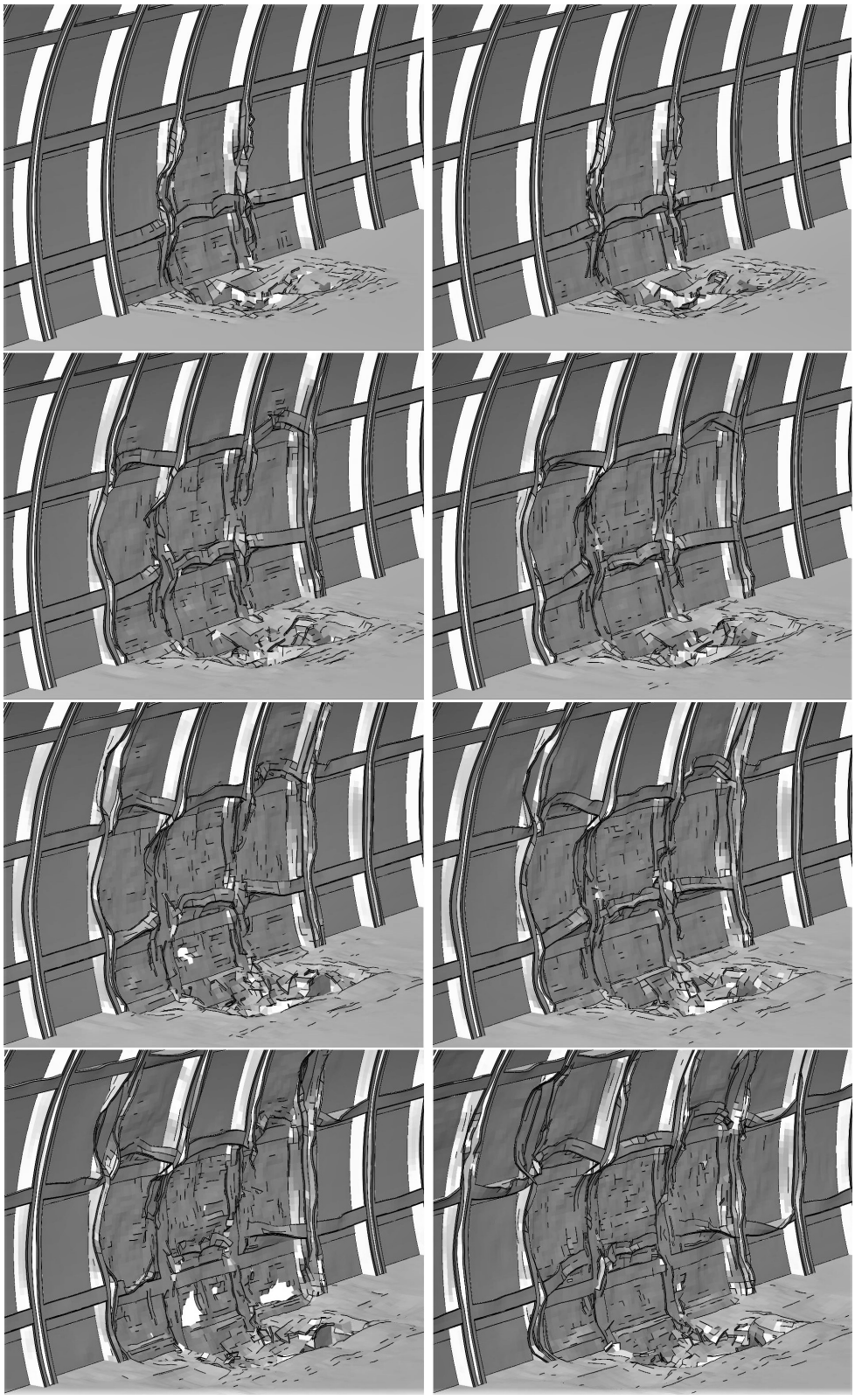

Fig. 25 Damage of the skin: case (a) (*left*) and case (b) (*right*).

References

[1] Gillen, D. and Morrison, W. G., "Aviation security: Costing, pricing, finance and performance," *Journal of Air Transport Management*, Vol. 48, 2015, pp. 1-12.

[2] Mlakar, P. F. and Klein, H. H. and Smith, J. L., "Hardened Unit Load Devices," *Proceedings FAA Aircraft Hardening and Survivability Symposium*, 1992, pp. 1-7.

[3] Sanai, M. and Greenfield, G. R., "Hardened Luggage Container," United States Patent US 5,267,665, 1993.

[4] Fray, J., "Venting a space to relieve pressure generated by an explosion," British Aerospace Public Limited Company 07/897,495, 1992.

[5] Hararat-Tehrani, M., "Decompression panel for a separation device in an aircraft," Deutsche Airbus Gmbh 07/626,888, 1992.

[6] Settles, G. S. and Keane, B.T and Anderson, B. W. and Gatto, J. A., "Shock waves in aviation security and safety," *Shock Waves*, Vol. 12, 2003, pp. 267-275.

[7] Backman, D. and Gould, R., "Blast Response of a Pressurized Aircraft Fuselage Measured Using High-Speed Image Correlation," *Experimental Techniques*, Vol. 39, 2015, pp. 4-9.

[8] Veldam, R. L. and Ari-Gur, J. and Clum, C., "Response of pre-pressurized reinforced plates under blast loading," *International Journal of Impact Engineering*, Vol. 35, 2008, pp. 240-250.

[9] Flight Safety Foundation, *Aviation safety database*, 2017, URL: `https://aviation-safety.net/`.

[10] Soutis, C. and Mohamed, G. and Hodzic, A., "Modelling the structural response of GLARE panels to blast load," *Composite Structures*, Vol. 94, 2011, pp. 267-276.

[11] Dacko, A. and Toczyski, J., "Vulnerability analysis of aircraft fuselage subjected to internal explosion," *The Arhive of Mechanical Engineering*, Vol. 58, 2011.

[12] Kotzakolios, T. and Vlachos, D. E. and Kostopoulos, V., "Blast response of metal composite laminate fuselage structures using finite element modelling," *Composite Structures*, Vol. 93, 2011, pp. 665-681.

[13] Masi, F., "Blast actions from high explosives. Studies on their simulation and effects," Master Thesis, University of Florence, Florence, 2017.

[14] Vannucci, P. and Masi, F. and Stefanou, I., "A study on the simulation of blast actions on a monumental structure," 2017, <hal-01447783v3>, URL: `https://hal.archives-ouvertes.fr/hal-01447783v3/document`.

[15] Jones, H. and Miller, A. R., "The detonation of solid explosives," *Proc. Royal Soc. A*, Vol. 194, 1948, pp. 480.

[16] Wilkins, M. L., "The equation of state of PBX 9404 and LX 04-01," Lawrence Radiation Laboratory, TID 4500 - UCRL 50422, CA (US), 1968.

[17] Lee, E. L. and Horning, H. C. and Kury, J. W., "Adiabatic expansion of high explosives detonation products," Lawrence Livermore National Laboratory, UCRL - 7797, Livermore, CA (US), 1964.

[18] Rogers, G.F.C. and Mayhew, Y.R., *Thermodynamic and Transport Properties of Fluids*, Wiley, 1988.

[19] Lee, E. and Finger, M. and Collins, W., "JWL equation of state coefficient for high explosives," Lawrence Livermore National Laboratory, UCID - 16189, Livermore, CA (US), 1973.

[20] USACE, "Design and Analysis of Hardened Structures to Conventional Weapons Effects," U. S. Army, TM 5-855-1, 1986.

[21] USACE, "Structures to Resist the Effects of Accidental Explosions," U. S. Army, TM 5-1300, 1990.

[22] USACE, "Structures to Resist the Effects of Accidental Explosions," U. S. Army, UFC 3-340-02, 2008.

[23] Karlos, V. and Solomos, G., "Calculation of Blast Loads for Application to Structural Components," Joint Research Center of the European Commission, JRC 32253-2011, 2013.

[24] Kingery, C. N. and Bulmash, G., "Air blast parameters from TNT spherical air burst and hemispherical burst," U.S. Army Ballistic Research Laboratory, ARBRL-TR-02555, 1984.

[25] Vannucci, P. and Stefanou, I. and Masi, F., "Cathédrales durables," CNRS, Final report, Paris (FR), 2017.

[26] Masi, F. and Stefanou, I. and Vannucci, P., "A study on the effects of an explosion in the Pantheon of Rome," Engineering Structures (submitted), 2017, <hal-01493006v1>, URL: `https://hal.archives-ouvertes.fr/hal-01493006/`.

[27] Johnson, G. and Cook, W. H., "A constitutive model and data for metals subjected to large strains, high strain rates and high temperatures," *Proceedings of the 7th International Symposium on Ballistics*, Vol. 21, The Hague, The Netherlands, 1983, pp. 541-547.

[28] Corona, E. and Orient, G. E., "An Evaluation of the Johnson-Cook Model to Simulate Puncture of 7075 Aluminum Plates," Sandia National Laboratories, SAND2014-1550 505013, Albuquerque, NM (US), Feb. 2014.

[29] Kray, G., "Failure modeling of titanium 6Al-4V and aluminum 2024-T3 woth the Johnson-Cook material model," Lawrence Livermore National Lab., UCRL-ID-149880, CA (US); Sep. 2002.

[30] ABAQUS (2016), "ABAQUS Documentation", Dassault Systèmes, Paris, FR.

[31] Zhu, G. and Glodsmith, W. and Dharan, C. K. H., "Penetration of laminated Kevlar by projectiles - I. Experimental investigation," *International Journal of Solids Structures*, Vol. 29, 1992, pp. 399-420.

[32] Cheeseman, B. A. and Bogetti, B. A., "Ballistic impact into fabric and compliant composite laminates,"

Composite Structures, Vol. 61, 2003, pp. 161-173.

[33] Hashin, Z., "Failure Criteria for Unidirectional Fiber Composites," *Journal of Applied Mechanics*, Vol. 47, 1980, pp. 329-334.

[34] Wang, Y. and Li, J. and Zhao, D., "Mechanical properties of fiber glass and Kevlar woven fabric reinforced composites," *Composites Engineering*, Vol. 5, 1995, pp. 1159-1175.

[35] Goods, S. H. and Neuschwanger, C. L. and Henderson, C. and Skala, D. M., "Mechanical properties and energy absorption characteristics of a polyurethane foam," Sandia National Laboratories, SAND97-8490 UC 404, Albuquerque, NM (US), Mar. 2014.